Interactions of polystyrene nanoplastics with *in vitro* models of the human intestinal barrier

Josefa Domenech[1], Alba Hernández[1,2], Laura Rubio[3] Ricard Marcos[1,2,#], Constanza Cortés[1,#]

[1]Grup de Mutagènesi, Departament de Genètica i de Microbiologia, Facultat de Biociències, Universitat Autònoma de Barcelona, Bellaterra, Spain; [2]Consortium for Biomedical Research in Epidemiology and Public Health (CIBERESP), Carlos III Institute of Health, Madrid, Spain. [3]Nanobiology Laboratory, Department of Natural and Exact Sciences, Pontificia Universidad Católica Madre y Maestra, PUCMM, Santiago de los Caballeros, Dominican Republic.

[#]Corresponding authors at: Grup de Mutagènesi, Departament de Genètica i de Microbiologia, Universitat Autònoma de Barcelona, Edifici Cn, Campus de Bellaterra, 08193 Cerdanyola del Vallès (Barcelona), Spain.

E-mail: constanza.cortes@uab.es (C. Cortés)

ricard.marcos@uab.es (R. Marcos)

alba.hernandez@uab.es (A. Hernández)

l.rubio@ce.pucmm.edu.do (L. Rubio)

josefa.domenech@uab.es (J. Domenech)

Running title: Nanoplastic effects in *in vitro* models of intestinal barrier

Abstract

Background: The universal presence of micro-nanoplastics (MNPLs) and their relative unknown effects over human health is a concern which demands reliable data to evaluate their safety. As their ingestion is one of the main exposure routes for humans, we have assessed their potential hazards by using two *in vitro* models simulating the human intestinal barrier and its associated lymphoid system.

Methods: Two different coculture models of differentiated Caco-2/HT29 intestinal cells and Caco-2/HT29 + Raji-B cells, presenting inherent human intestinal epithelium characteristics were exposed to nanopolystyrene (NPS) for 24 h. Different endpoints such as viability, membrane integrity, NPS localization and translocation, ROS induction, and genotoxic damage were evaluated to have a wide comprehensive view of their potentially harmful effects.

Results: No significant cytotoxic effects were observed in any of the assayed systems. In addition, no adverse effects were detected neither in the integrity of the barrier models nor in their permeability. Nevertheless, confocal microscopy analysis showed that MNPLs were uptaken by both of the barrier model systems and that translocation across the membrane occurred, as MNPLs were also detected inside Raji-B cells, placed in the baso-lateral compartment of the insert. The internalization seemed to have a dose-dependent pattern, as assessed by flow cytometry. Nonetheless, no genotoxic or oxidative DNA damage induction was detected in either case. Finally, no variations in the transcription of oxidative and stress genes could be detected in any of the *in vitro* barrier models.

Conclusions: Our results show that exposure to MNPLs can enter and cross the epithelial barrier of the digestive system, but they do not have a hazardous effect, according the used biomarkers.

Keywords: Nanoplastics; Styrene nanoparticles; Intestinal barrier; Caco-2/HT29/Raji-B cells.

Introduction

Thanks to their paramount characteristics, including low production cost, plastics are widely used for multiple types of applications. The amount produced per year is extremely high: according to the Plastics Europe consortium, 335 million tons of the different types of plastic were fabricated in the world in 2016, a significant part of which (60 million tons) was manufactured in Europe (PlasticsEurope, 2017).

Since the majority of the plastics produced is for single-use, large amounts of plastic litter are released into the environment, resulting in an important environmental concern. The impact of marine plastic waste is particularly relevant, as it seems to be ubiquitous in both coastal areas and the open sea (Li et al., 2016), as well as in the subtropical gyres that represent the main accumulation hot spots (Eriksen et al., 2013). Although macroplastic litter represents the visible face of plastic pollution, it is subjected to constant degradation, leading to its transformation into micro- and nanoplastics (MNPLs) (Lambert y Wagner, 2016; Ioakeimidis et al., 2016). Thus, MNPLs represent not only an environmental challenge but also a potential human health risk factor.

Most of the plastics produced by the industry are composed of different types of synthetic polymers such as polyethylene, polypropylene, and polystyrene, among others. Accordingly, such synthetic polymers are present in the environmental plastic litter and, consequently, in the resulting MNPLs (Hidalgo-Ruz et al., 2012). Notwithstanding, MNPLs not only result from the degradation of plastic debris but the industry also produces micro- and nano-sized plastics used for different purposes like the exfoliating agents present in personal care products such as creams (Silva et al., 2018). Regardless of their origin, all types of MNPLs will be finally present in different environmental matrices.

It is assumed that ingestion is the principal exposure route present in marine organisms as MNPLs have been widely detected in their digestive tracts (Carbery et al., 2018). Furthermore, the MNPLs' size range facilitates their translocation through the gastro-intestinal membranes via endocytosis-like mechanisms and their following distribution to different tissues and organs (Alimba and Faggio, 2019). Since MNPLs can bioaccumulate

through the trophic web, humans are most likely exposed by the consumption of marine organisms. This means that the potential health risk that MNPLs pose to humans beings needs to be urgently analyzed (Wright et al., 2017; Rist et al., 2018). However, it must be remembered that the consumption of marine organisms constitutes only a part of the potential human intake of MNPLs. Given the ubiquitous nature of MNPLs, many sources and routes of exposure are foreseeable, including inhalation due to the presence of MNPLs in the air of urban areas (Prata et al., 2018; Klein and Fischer, 2019). Although the information regarding human exposure to MNPLs continues to grow, the low number of studies aiming to evaluate the potential health effects of MNPLs in humans is alarming. Thus, new studies using different human cells models are required.

As ingestion is considered one of the most relevant exposure routes to MNPLs for humans, the evaluation of the potential interactions between MNPLs and the human intestinal barrier is necessary. For this purpose, *in vitro* gut models based on the use of Caco-2 cells have been largely proposed. These human colorectal adenocarcinoma cells can differentiate forming a morphologically and functionally enterocyte-like monolayer (Sambuy et al., 2005). To better mimic the complex environment of the human intestine, where other cells types exist, different modifications of the original monoculture model have been proposed, such as the coculture of Caco-2 and HT29 cells. HT29 are goblet-like cells capable to secrete vacuoles full of mucin, conferring an extracellular protective mucus shed (Araújo and Sarmento, 2013; Lozoya-Agullo et al., 2017). Furthermore, another improvement of the monoculture system proposes the addition of lymphoblast-like Raji-B cells to the complex Caco-2/HT29 coculture in the basolateral chamber of the insert where Caco-2/HT29 grow, inducing the differentiation of Caco-2 cells into M-like cells. Microfold cells (M cells) are antigen sampling cells which promote particle transcytosis acting as the gateway for antigens from the gut lumen (Kucharzik et al., 2000). Also, it is important to remark that different types of nanoparticles have been proven to cross the intestinal epithelium mainly via M-cells (des Rieux et al., 2005).

In this context, we have evaluated the interaction of polystyrene nanoparticles (PSNPs) with

both Caco-2/HT29 and Caco-2/HT29/Raji-B coculture models to visualize the potential *in vivo* interactions that could take place. In addition to using pristine PSNPs, we have used the same nanoparticles conjugated to fluorophores to better follow the fate of the PSNPs in our model. This allows the detection of PSNPs by their fluorescence. Besides the uptake of PSNPs by the barrier, we have evaluated their potential translocation, changes in the barrier's stability and integrity, and the induction of oxidative stress and genotoxicity.

.

Materials and Methods

Cell culture and differentiation of the in vitro barrier models

Three different human cell lines, namely Caco-2, HT29, and Raji-B, have been used. The human colorectal adenocarcinoma-derived cell line Caco-2 was provided by Dr. Isabella Angelis (Istituto Superiore di Sanità, Italy). The HT29 cell line is also a human cell line derived from colorectal adenocarcinoma. The Raji-B cell line is a lymphoblast-like cell line established from a human Burkitt's lymphoma. Both HT29 and Raji-B cell lines were acquired from the American Type Culture Collection (ATCC, Manassas VA 20108, USA). All the three cell lines were maintained in Dulbecco's modified Eagle's High Glucose medium (DMEM) without sodium pyruvate (Biowest, France) supplemented with 10% fetal bovine serum (FBS), 1% non-essential amino acids (NEAA) (Biowest, France), 1% Amphotericin B (Biowest, France) and 2.5 µg/mL Plasmocin (Invivo Gen, San Diego, CA). Cells were cultured in a humidified atmosphere of 5% CO_2 and 95% air, at 37 ºC. Routinely, Caco-2 and HT29 cells were subcultured twice a week at 70% confluence, dispersing them with 1% trypsin-EDTA (Biowest, France). Raji-B cells were grown in suspension and subcultured by dilution twice a week.

For the formation and differentiation of the Caco-2/HT29 *in vitro* barrier model, a total of 1.7 x 10^5 Caco-2 and HT29 cells were seeded at a 90:10 ratio on 1.12 cm^2 polyethylene terephthalate (PET) Transwell® membranes with 1 µm pores (Merck KGaA, Darmstadt, Germany) in 12-well plates (García-Rodríguez et al., 2018a). To obtain a well-differentiated barrier, cocultured cells were grown for 21 days. To establish the Caco-2/HT29/Raji-B model of *in vitro* barrier, 5 x 10^5 Raji-B cells were added to the basolateral side at day 14 of the Caco-2/HT29 barrier differentiation, for the M-like cell induction (García-Rodríguez et al., 2018b). Cultures were extended until day 21. In both models, the culture medium was changed every two days.

Dispersion and characterization of polystyrene nanoparticles

Two commercial types of PSNPs were used: pristine and fluorescent nanoparticles. Both types were obtained from Spherotech (Chicago, USA). Pristine PSNPs (nPSNPs, PP-008-10), with a nominal size ranging from 0.05 to 0.1 μm, were used in all the experiments. Fluorescent yellow PSNPs (y-nPSNPs, FP-00552-2), with a nominal size ranging from 0.04 to 0.09 μm, were used in the experiments analyzing cellular uptake or barrier translocation. PSNPs dispersions were diluted to 100 μg/mL in distilled water or DMEM and further characterized by transmission electron microscopy (TEM), using a JEOL JEM-1400 instrument (Jeol LTD, Tokyo, Japan). Additionally, both the hydrodynamic size and the Z-potential parameters were evaluated using dynamic light scattering (DLS) and laser Doppler velocimetry (LDV) methodologies, in a Malvern Zetasizer Nano ZS zen3600 device (Malvern, UK).

Exposure to polystyrene particles

To assess the biological effects induced by PSNPs, differentiated Caco-2/HT29 or Caco-2/HT29/Raji-B barriers were exposed to 0, 1, 25, 50 and 100 μg/mL of nPSNPs (or y-nPSNPs) for 24 h on the 21st day of the differentiation process. PSNPs dispersions were prepared by diluting the original stock in DMEM culture medium to reach the desired concentrations, and the apical medium of the cultures (transwells) was replaced by 1 mL of the different selected PSNPs concentrations.

Determination of cell viability after PSNPs exposure

To determine the toxic effects of PSNPs concentrations we determined cell viability by using the Beckman counter method, with a ZTM Series coulter-counter (Beckman Coulter Inc., USA). This determination was carried out using nPSNPs only, to select the range of doses to be used in the study. Since our interest is the evaluation of the effects induced by nPSNPs we did not extend these preliminary toxicity studies to the fluorescent y-nPSNPs. The *in vitro* models of Caco-2/HT29 and Caco-2/HT29/Raji-B were exposed to nPSNPs for 24 h using the following concentrations: 0, 25, 50, 100, 125, 150, 175 and 200 μg/mL. After the exposure

time, treatments were removed and monolayers were washed with PBS 1X before detaching them with trypsin-EDTA 1%. After this step, trypsin was inactivated with PBS containing 2% of FBS. Finally, the mixture of cells was diluted 1:100 in ISOTON™ (Beckman Coulter™, ref no. 844 80 11, USA) to be counted in the Beckman counter. In a like manner, Raji-B cells seeded in the basolateral chamber of the Caco-2/HT29 + Raji-B model were collected, diluted 1:100 in ISOTON™, and counted in the Beckman counter.

Evaluation of the barrier's integrity

The integrity of the Caco-2/HT29 barriers was assessed by measuring the transepithelial electrical resistance (TEER) of the monolayers in both used models. An epithelial voltmeter, Millicell-ERS volt/ohm meter (Merck KGaA, Darmstadt, Germany), was used to perform the TEER measurements. Briefly, treatments were removed 24 h after the exposure, the apical compartments of the models were washed thrice with PBS 1X, and fresh DMEM was added. Also, the basolateral compartments were emptied, washed, and DMEM or Raji-B cells were replaced by fresh DMEM cell culture. Measures were taken in two different parts of the insert from each sample. TEER values were determined according to the formula TEER = [Ω (cell inserts) – Ω (cell-free inserts)] x 1.12 cm^2. Additionally, both *in vitro* models were treated with 20 mg/mL benzalkonium chloride (Sigma Aldrich, Germany) for 40 min at 37 ºC, as a positive control.

Paracellular permeability assessment

The paracellular transport of Lucifer yellow (LY) (ThermoFisher Scientific, USA) was evaluated to assess the barrier's permeability after the exposure to nPSNPs. Briefly, treatments were removed from the apical compartment of the *in vitro* systems and the Caco-2/HT29 barriers were washed thrice with Hank's balanced salt solution (HBSS) (Ca^{2+}, Mg^{2+}, 10 mM HEPES [4-(2-hydroxyethyl)-1-piperazineethanesulfonic acid], pH 7.4) (Sigma-Aldrich, Germany). The basolateral DMEM cell culture medium, or Raji-B cells, were also removed from the basolateral chamber and the Transwells® were washed with HBSS. Then,

Transwells® were transferred to a clean 12-well plate, each well containing 1.5 mL of HBSS, and 0.5 mL of 0.4 mg/mL of LY in HBSS was added to the apical side of the models. After incubating the system for 2 h at 37 ºC, each basolateral sample was analyzed to quantify the amount of LY. The LY fluorescence, as indicative of the LY that was able to cross the barrier, was measured at 405-535 nm as excitation-emission spectrum with a fluorimeter (Victor III, Perkin Elmer, USA). Cell-free inserts were used as a positive control, as well as samples treated with 20 mg/mL of benzalkonium chloride (Sigma Aldrich, Germany) for 40 min at 37 ºC.

Determination and quantification of cellular uptake of y-nPSNPs

To determine the localization of PSNPs, Caco-2/HT29 and Caco-2/HT29 + Raji-B *in vitro* models were treated with y-nPSNPs. After the exposure time, treatments were removed and barriers were washed twice with DMEM. Caco-2/HT29 monolayers were stained for 15 min at room temperature with the nucleus dye Hoechst 33342 (1:500 in DMEM) (ThermoFisher Scientific, USA), and the cell membrane and mucus dye Cellmask™ Deep Red plasma (1:500 in DMEM) (Life Technologies, USA). Transwells were then cut and mounted in a MatTek Glass Bottom Dish (MatTek, USA) with a mounting medium drop. Regarding the Caco-2/HT29 + Raji-B model, 0.5 mL of basolateral medium containing Raji-B cells were collected and incubated with Hoechst 33342 (1:500 in DMEM) and Cellmask™ Deep Red plasma (1:500 in DMEM) for 5 min at room temperature. Samples were dropped in a Menzel-Gläser Polysine adhesion slides (Thermo-Scientific, USA) and covered with a coverslip. Confocal images were acquired with a Leica TCS SP5 confocal microscope (Leica, Germany). y-nPSNPs were visualized thanks to the yellow fluorophore they incorporate. IMARIS 9.2 software was used to analyze and process the images obtained.

Additionally, y-nPSNPs uptake by the Caco-2/HT29 barriers and the Raji-B cells was quantified using flow cytometry. Briefly, after the exposure to y-nPSNPs, Caco-2/HT29 monolayers were washed twice with PBS 1X and trypsinized. Cells were then resuspended in PBS 1X to obtain $1x10^6$ cells/mL in a FACS tube and samples were kept on ice. 1:1000

propidium iodide was added 5 min before the analysis by flow cytometry to determine cell viability. On the other hand, Raji-B cells from de Caco-2/HT29 + Raji-B model were collected after the exposure time to y-nPSNPs, centrifuged, and resuspended to obtain $1x10^6$ cells/mL. Samples were kept on ice and 1:1000 propidium iodide was added before the analysis. A BD-FACSCanto Flow Cytometer (BD Bioscience, USA) was used in to determine the percentage of living cells containing y-nPSNPs and the relative cell fluorescence of the entire population of living cells in each sample.

Detection of intracellular ROS

The dichloro-dihydro-fluorescein diacetate (DCFH-DA) method was used to analyze the production of intracellular ROS. After the treatment and subsequent washing of the Caco-2/HT29 monolayers, belonging to the two different models studied, cells were resuspended in 20 µM DCFH-DA (Sigma-Aldrich, Germany) in serum-free DMEM. An hour later, a fluorimeter (Victor III, Perkin Elmer, USA) was used to measure the fluorescence at 490-535 nm as excitation-emission spectrum. A treatment with 100 mM H_2O_2 for 1 h was used as a positive control.

In addition, the production of intracellular ROS was also measured by the dihydroethidium (DHE) method. Once the exposure time to nPS was over, Caco-2/HT29 monolayers of both *in vitro* models (Caco-2/HT29 and Caco-2/HT29 + Raji-B) were washed, trypsinized, and centrifuged at 1,000 rpm for 5 min. Cells were then resuspended in 10 µM DHE in PBS 1X to a final concentration of $1x10^6$ cells/mL, and the DHE was incubated at 37 ºC for 30 min. From this point, samples were kept on ice. Before analyzing the samples, they were incubated with 3 nM VPR (Via-Probe™ Red Nucleic Acid Stain, BD Bioscience, USA) for 5 min in order to determine cell viability. 20,000 events were analyzed from the living-cells population with a BD-FACSCanto Flow Cytometer (BD Bioscience, USA). Samples exposed to 100 µg/mL cigarette smoke condensate (CSC) (Murty Pharmaceuticals, USA) for 45 min were used as positive control.

Determination of genotoxic and oxidative DNA damage

To assess the genotoxic damage (DNA breaks) and the oxidative DNA damage (ODD) in the Caco-2/HT29 barriers, after being exposed to nPSNPs, we used the alkaline comet assay supplemented with the use of formamidopyrimidine DNA glycosylase (FPG) enzyme. After the exposure to the different doses of nPSNPs, the apical and basolateral medium was removed, and the Caco-2/HT29 barriers were washed with PBS 1X and trypsinized; the resulting cell suspensions were centrifuged at 1,800 rpm for 8 min. Then, cells were resuspended in PBS 1X to a cellular density of $1x10^6$ cells/mL, mixed 1:10 with 0.75% low melting point agarose at 37 ºC, and, finally, triplicates of the samples were dropped on GelBond® films (GBF) (Life Sciences, Lithuania). GBF were incubated in cold lysis buffer overnight at 4 ºC and washed twice with enzyme buffer for 5 and 50 min, respectively, at 4 ºC. GBF were then incubated with or without FPG enzyme in enzyme buffer 1:25,000 for 30 min at 37 ºC, followed by the incubation in electrophoresis buffer for 35 min at 4 ºC to unwind DNA and expose the alkali-labile sites. The electrophoresis was carried out at 20 V and 300 mA at 4 ºC for 23 min. Finally, samples were washed with cold PBS 1X, fixed with absolute ethanol, and GBF were air-dried overnight at room temperature. To analyze the percentage of DNA in the comets' tail, cells were stained with SYBR Gold in TE buffer (1:10,000) for 20 min at room temperature, and GBF were mounted to visualize the samples in an epifluorescent microscope (Olympus BX50) at 20 magnifications. The quantification of the genotoxic damage and the ODD was done as the percentage of DNA in the comet's tail, with the Komet 5.5 Image analysis system (Kinetic Imaging Ltd, UK). The experiment was performed thrice, with duplicates for each treatment condition, and one hundred randomly-selected comet images were analyzed per each sample. 200 µM MMS and 5 mM $KBrO_3$ were used as a positive control for the genotoxic damage and the ODD, respectively.

Analysis of gene expression by Real-Time RT PCR

The expression of different genes (*Heme-oxygenase 1* (*HO1*), *Glutathione S-transferase P* (*GSTP1*), *Heat shock protein 70* (*HSP70*), and *Superoxide dismutase 2* (*SOD2*)) was

analyzed by Real-Time Reverse Transcription PCR (Real-Time RT PCR). After the exposure to nPSNPs of the Caco-2/HT29 and the Caco-2/HT29 + Raji-B models, membranes were washed with PBS 1X and the total RNA was isolated from the Caco-2/HT29 monolayers using TRI Reagent® (Sigma-Aldrich, Germany). Then, samples were treated with RNase-free DNase I (Turbo DNA-free kit; Invitrogen, USA) to discard DNA contamination, and cDNA was obtained by retrotranscription with the High Capacity RNA-to-cDNA kit (Applied Biosystems, USA). The obtained cDNA was analysed by Real-Time RT PCR on a LightCycler-480 (Roche, Basel, Switzerland). The expression of the *ß-actin* housekeeping gene was also analysed to eliminate the variability due to sample loading. The sequences of the primers used are indicated in Table 1.

Statistical analysis

All data resulted from the average of two independent experiments, including duplicates of each one of them, unless stated otherwise. Data were analyzed using GraphPad Prism 7 software, and statistical analysis was performed using the one-way ANOVA with a Dunnett post-test unless stated otherwise. Statistical significance was defined as a $*P \leq 0.05$, $**P \leq 0.01$, $***P \leq 0.001$.

Results

PSNPs dispersion and characterization

According to the supplier (Spherotech, Chicago, USA), both nPSNPs and y-nPSNPs present nominal sizes ranging from 0.05 to 0.1 µm and 0.04 to 0.09 µm, respectively. We used transmission electron microscopy (TEM) to confirm these sizes and morphologies. Figure 1 shows that both nanomaterials are round-shaped particles when diluted in distilled water or DMEM. Regarding their sizes, the average diameter of 100 randomly-selected particles was around 50 nm for both PSNPs in water or DMEM, as indicated in Table 2. Additional parameters were determined using a Zetasizer Nano ZS device, and the results are indicated in Table 2. When PSNPs were dispersed, the hydrodynamic sizes were bigger in DMEM than in water, suggesting the agglomeration of nanoparticles in culture medium. The Z-potential values corroborate this, as the electrokinetic potential measurements reflect higher stability in water-dispersed particles, confirming what was observed by TEM. Finally, the poly-dispersion index (PDI) values were close to zero, suggesting that samples were monodispersed.

Cytotoxicity assessment

Caco-2/HT29 and Caco-2/HT29 + Raji-B models were exposed to 0-200 µg/mL of nPSNPs to detect their cytotoxic potential. The obtained percentage values (Figure 2) constitute an average of the surviving number of cells of each treatment, compared to the untreated control cultures. The exposure of both *in vitro* models to nPSNPs for 24 h does not elicit any type of cytotoxicity neither in the Caco-2/HT29 monolayers of both models nor the Raji-B cells from the Caco-2/HT29 + Raji-B model. According to these results, we used 0, 1, 25, 50 and 100 µg/mL doses in subsequent experiments.

Effects of nPSNPs on the barrier's integrity

To assess the functional integrity of the barriers, TEER values of the Caco-2/HT29 and Caco-2/HT29 + Raji-B barrier models were measured after 24 h of exposure to nPSNPs.

Considering that TEER values above 300 Ω/cm^2 indicate a good condition of the membranes, we could not detect a significant decrease in the integrity of the barriers after the treatments under any nPSNPs exposure concentration. This was true for both the Caco-2/HT29 and the Caco-2/HT29 + Raji-B models (Figure 3). However, benzalkonium chloride, used as a positive control, lead to a very drastic decrease in the TEER values.

Effects of nPSNPs on barrier's permeability

To determine the permeability status of the barrier, we analyzed the LY flux through monolayers previously treated with nPSNPs. As shown in Figure 4, we could not detect a significant increase in the levels of LY in the basolateral chamber after exposures to nPSNPs lasting for 24 h. Accordingly, the permeability of the Caco-2/HT29 barriers of both models, Caco-2/HT29 (Figure 4A) and Caco-2/HT29 + Raji-B (Figure 4B), remained intact after exposures. On the other hand, the benzalkonium chloride positive control was able to disrupt the Caco-2/HT29 monolayers leading to a significant accumulation of LY to the basolateral side, an effect also observed in the cell-free inserts.

Determination and quantification of cellular uptake of y-nPSNPs

Confocal microscopy was used to localize y-nPSNPs inside the cells forming the Caco-2/HT29 barriers, and in the Raji-B cells taking advantage of the nanoparticles' fluorescent properties (Figure 5). y-nPSNPs were found inside the cells forming the Caco-2/HT29 monolayers at all the concentrations assayed. Moreover, nanoparticles were detected inside the nuclei of the cells forming the barrier, independently of the concentration tested.

On the other hand, for the Caco-2/HT29 + Raji-B cells *in vitro* model, y-nPSNPs uptake was analyzed after the exposure in both the barrier and in the Raji-B cells placed in the basolateral compartment. In this model, we were also able to find y-nPSNPs inside the monolayers' cytoplasm, and in their nuclei, at all the doses tested. Regarding Raji-B cells, although uptake was observed at all the tested concentrations, y-nPSNPs were only detected in the nuclei of cells belonging to samples exposed to the highest dose assayed of 100 µg/mL. These results

indicate that y-nPSNPs were able to enter the cells forming the barrier of the Caco-2/HT29 + Raji-B model, and reaching the nuclei of the monolayers' cells. Furtherly, some y-nPSNPs were able to completely cross the barrier and translocate to the basolateral space of the system. Here, they were internalized by the Raji-B cells, even entering their nuclei at the highest dose assayed.

To quantify the PSNPs uptaken by the Caco-2/HT29 monolayers and the Raji-B cells from both models, the percentage of fluorescent cells, as well as the fluorescence intensity in each cell, were assessed by flow cytometry. On the one hand, significant differences with the untreated controls in the percentage of fluorescent-positive living cells were observed at all the doses assayed in both Caco-2/HT29 monolayers from the Caco-2/HT29 and the Caco-2/HT29 + Raji-B models, as well as in the Raji-B cells (Figure 6, A-C, respectively). Starting from 1 μg/mL, fluorescent cells reached about 15% of the examined population in the Caco-2/HT29 monolayers. The percentage of cells that uptook y-nPSNPs continued to increase in a dose-dependent manner, reaching about 60% of the living cells for the Caco-2/HT29 model and the Raji-B cells, and 75% of the examined population for the monolayers belonging to the Caco-2/HT29 + Raji-B model, at the highest concentration assayed. The flow cytometry assay was also used to assess the mean fluorescence emission of fluorescent-positive living cells in the different samples analyzed. The results obtained showed that there were significant differences compared to the untreated control at all the doses assayed for both kinds of Caco-2/HT29 monolayers, as well as for Raji-B cells (Figure 6, A'-C', respectively). The differences in the mean fluorescence emission were about thirty times higher for the Caco-2/HT29 monolayers of the different models studied exposed to 100 μg/mL, and six times higher in the Raji-B cells belonging those samples.

Production of intracellular ROS

The intracellular generation of ROS was measured by using two different approaches: the DCFH-DA and the DHE assays. DCFH-DA has a wider ROS spectrum reacting with H_2O_2, $ONOO^-$, lipid hydroperoxides and, to a lesser extent, with superoxide. On the other hand,

DHE reacts mainly with the latter. Thus, using these two assays the main panel of intracellular ROS is covered.

The levels of intracellular ROS in the Caco-2/HT29 barriers of the Caco-2/HT29 and Caco-2/HT29 + Raji-B models were measured after the exposure to nPSNPs with the DCFH-DA assay. The production of intracellular ROS was quantified from the fluorescence intensity detected for each sample. As shown in Figure 7 A and B, we could not find significant ROS production at any dose in the Caco-2/HT29 barriers of both models assayed. However, monolayers exposed to positive control, H_2O_2, showed a great increase in the fluorescence intensity, indicating an increase in the intracellular ROS production. When intracellular ROS induction was analyzed by the DHE assay (Figure 7 C and D) in the Caco-2/HT29 monolayers of the models assayed also negative results were obtained. Thus, we did not detect production of intracellular ROS at any dose tested for any of the models assayed, Caco-2/HT29 and Caco-2/HT29 + Raji-B. Despite that, the positive control (CSC) produced a significant increase in the ROS production.

Genotoxic and oxidative DNA damage

To determine the genotoxic and oxidative DNA damage in the monolayers of the Caco-2/HT29 and Caco-2/HT29 + Raji-B models, after the exposure to nPSNPs, the alkali comet assay complemented with the FPG enzyme was used. As shown in Figure 8A, the percentage of DNA in the tail found in the cells of the Caco-2/HT29 model exposed to nPSNPs was not significantly higher than the one observed in the untreated samples. However, the suitability of the assay is supported by the data obtained for those samples treated with the 200 µM MMS positive control, showing a high increase in the percentage of DNA in the tail. Regarding ODD (Figure 8A'), the version of the comet assay supplemented with the FPG enzyme did not show significant changes in the percentage of DNA in the tail between the untreated and treated samples, unlike the samples exposed to the 5 mM $KBrO_3$ positive control, which showed a significant increase in the levels of ODD.

On the other hand, the genotoxic and the ODD damage from the Caco-2/HT29 barriers belonging to the Caco-2/HT29 + Raji-B showed no significant genotoxic damage in the barriers of the Caco-2/HT29 + Raji-B model at any of the assayed concentrations (Figure 8B). Also, when we performed the modified version of the comet assay with the addition of the FPG enzyme, the percentage of DNA in the comets' tail did not increase at any of the conditions analyzed (Figure 8B'). However, a significant increase in both the genotoxic damage and the ODD was observed when the barriers were exposed to their respective positive controls.

Analysis of gene expression by Real-Time RT PCR

Changes in the expression of genes associated with different cellular stress pathways were analysed by Real-Time RT PCR in the Caco-2/HT29 monolayers, from both the assayed models. On the one hand, we could not detect significant changes in the expression of the three ROS-related genes analysed (*HO1, GSTP1,* and *SOD2*) nor in the levels of *HSP70* gene, which is an indicator of general cellular stress induction in the Caco-2/HT29 *in vitro* model. However, a slight tendency to increase the expression of these genes in a dose-dependent manner can be seen in Figure 9A. Regarding the Caco-2/HT29 + Raji-B *in vitro* model (Figure 9B), we could not detect significant changes in the expression of the genes analyzed, but again, we detect an increasing tendency to higher levels of expression at higher doses of nPSNPs, especially for the cellular stress indicator *HSP70*.

Discussion

The obvious presence of plastic wastes in sea waters seems that, finally, it is drawing the attention of media, policymakers, and general population about this dramatic environmental problem. Nevertheless, this visual impact of environmental plastic wastes hides a more important problem associated with the small sized plastics resulting from the degradation of the large-sized plastic materials. Thus, plastics sized at the micrometric and nanometric size are polluting not only the seas but all types of environments. Although a large amount of scientific effort has been dedicated to understanding the environmental effects of MNPLs, the comprehension of the human health impact remains largely unknown (Toussaint et al., 2019).

As the problem emerged in the sea, and plastics could reach humans trough the trophic web, the first approaches aimed to confirm the trophic transfer of MNPLs in the marine food web. Although there are many studies showing that MNPLs are transferred along trophic levels, it is no clear if bioaccumulation and/or biomagnification processes take place (Santana et al., 2017; Carbery et al., 2018). Thus, there is an important lack of information on the potential transfer of MNPLs from seafood to humans, and their implications for human health.

A second question was if MNPLs remained in the gut, or spread over the different organs and tissues, following translocation through the intestinal barrier. The answer to this question has important implications because for many fish species the gut is not an edible part, and it is removed before consumption. Thus, if MNPLs do not translocate through the intestinal barrier the exposure for humans, associated to fish consumption would be very low. Nevertheless, many marine organisms like mussels are eaten without eliminate the intestine. As for many nanomaterials, the low size of MPLs, and specially NPLs, facilitate their ready translocation through the intestinal barrier and accumulate in tissues and circulatory system of aquatic species (Auta et al., 2017; Su et al., 2019). Accumulation studies in mammals are lacking with the exception of the pioneering study of Deng et al. (2017). In that study bioaccumulation was reported in mice using fluorescent polystyrene MPLs sized 5 and

20 µm, and both sizes of MPLs were detected in the liver, kidney, and gut. Interestingly, this study observed an increased bioaccumulation over time.

Accordingly, and to better understand the interactions of NPLs with the intestinal barriers we have used the *in vitro* model of differentiated Caco-2 cells cocultured with HT29 cells or with HT29 + Raji-B cells. Since HT29 are goblet-like cells capable to secrete mucin, they confer an extracellular protective mucus shed to the barrier (Lozoya-Agullo et al., 2017). Furthermore, the addition of lymphoblast-like Raji-B cells induces the differentiation of Caco-2 cells into M-like cells. Microfold cells (M cells) are antigen sampling cells having a high capacity for particle transcytosis representing a weak point in the intestinal barrier (Kucharzik et al., 2000). Using both models we have been able to demonstrate the easy uptake of PSNPs by the barrier, as well as their translocation from the apical to the basolateral side.

Interestingly, the exposure to PSNPs does not induce apparent toxicity to the cells constituting the intestinal barrier model. These results would confirm the indicated by other authors who did not detect any cytotoxic effect of fluorescent PETNPs in monolayers of Caco-2 cells (Magrì et al., 2018). Similar results were obtained also, but in undifferentiated Caco-2 cells, testing the effects of PSMNPLs (0.1 and 5 µm), where mild changes in membrane integrity and negligible changes in its fluidity were observed. Interestingly, the effects induced by the larger size (5 µm) were higher than those induced by 0.1 µm sizes (Wu et al., 2019). In addition, two very recent studies using COOH-modified PSMNPLs (50 nm and 0.5 µm) in the co-culture (Caco-2/HT29-MTX-E12), and using fluorescent PSMPLs (1.4 and 10 µm) in the co-culture (Caco-2/HT29-MTX-E12/Raji-B), did not found relevant toxic effects (Stock et al., 2019; Hesler et al., 2019). These negative toxic effects obtained in Caco-2 cells agree with those reported using other human cells lines as cerebral (T98G) and epithelial (HeLa) human cells (Schirinzi et al., 2017), human macrophage THP-1 cells (Stock et al., 2019), and in placental trophoblast (BeWo b30) cells (Hesler et al., 2019). Nevertheless, these negative results differ from those reported in the human lung epithelial BEAS-2B cells were the MTS assay showed a dose-dependent significant decreased in cell viability after exposures to PSNPLs, where positive effects were detected at concentrations up 10 µg/mL (Lim et al.,

2019). In addition to the lack of toxicity of nPSNPs, on the cells constituting our intestinal barriers models, we have demonstrate the neither the barrier integrity not the barrier permeability were affected by PSNPs exposures. These approaches were also used in the two studies using of Caco-2 or cocultures (Stock et al., 2019; Hesler et al., 2019). Interestingly, no changes in the TEER values were detected in these studies confirming our findings.

It should be pointed out that, in spite of the low toxicity of pristine MNPLs, in the environment they can act as a potent vectors for heavy metals and organic pollutants (Lin et al., 2019; Bradney et al., 2019). The adsorption of these compounds by MNPLs may be facilitated by their high surface area and its functionalization, as well by environmental conditions such as pH and water salinity (Bradney et al., 2019). Although this is not the topic of this study it is obvious that this potential role as a carrier need further research.

Despite the absence of toxicity, PSNPs were able to be easily uptaken by the barrier models, as detected by using fluorescent labelled PSNPs. This easy uptake has been observed in undifferentiated Caco-2 cells (Magri et al., 2018) or in cocultures. (Stock et al., 2019; Hesler et al., 2019). Regarding the translocation thought the barrier, this parameter was not tested in one of the studies using cocultures (Hesler et al., 2019), and the levels observed in the basolateral size were below the limit of detection in the other one (Stock et al., 2019). Interestingly, significant translocation was observed using PETNPs with a time-dependent increase of particles in the basolateral compartment (Magri et al., 2018). In our study, the presence of Raji-B cells in the basolateral compartment was used to detect its uptake of y-nPSNPs. This approach never has been used in the studies using *in vitro* models of intestinal barriers, and testing MNPLs effects. This model mimicry pretty well what occurs *in vivo* where, once the barrier has been crossed, MNPLs can interact with lymphoid cells as it is the case of Raji-B cells. Thus, our results show a potential route of spreading MNPLs among the different organs, after ingestion.

Among the different biological effects caused by environmental pollutants and nanoparticles, and by extension by MNPLs, stand up the induction of intracellular oxidative stress. In fact,

the involvement of oxidative stress as possible mechanisms of MNPLs induced toxicity in marine organisms has been proposed (Alimba and Faggio, 2019), although contradictory results have been reported. In mammalian cells a slight potential of PE- and PSMNPLs to disturb homeostasis at oxidative cellular level in cerebral and an epithelial cell lines was reported (Schirinzi et al., 2017). Furthermore, oxidative stress induction was also observed in human dermal fibroblasts and in murine macrophages exposed to PSMNPLs (0.1 and 5 μm), but only when the smaller size was used (Wu et al., 2019). In differentiated Caco-2 cells the studies of Stock et al. (2019) and Hesler et al. (2019), who evaluated the biological effects of PSMNPLs, did not measure the potential induction of oxidative stress. Nevertheless, in undifferentiated Caco-2 cells PSMNPLs exposure induced mild oxidative damage induction (Wu et al., 2019). Interestingly, in the monoculture of differentiated Caco-2 cells Magri et al. (2018) did not detect the induction of oxidative stress by PETMNPLs. These negative results would agree with our data showing no induction of oxidative stress by PSNPs exposure. It should be remembered that, due to the contradictory literature data we carried out two different experiments (DCFH-DA and DHE methods) measuring intracellular ROS induction. The use of two different assays to measure the oxidant potential of PSMNPLs gives special strength to the obtained results. Thus, although both assays determine intracellular ROS, each one reacts with different reactive molecules. While DCFH-DA penetrates cell membranes and reacts with H_2O_2, $ONOO^-$, lipid hydroperoxides and, to a lesser extent, with superoxide, DHE reacts mainly with the latter. Thus, the use of these two assays cover the main panel of intracellular ROS, and its combination is a good choice to full analyze the effect of MNPLs in oxidative scenarios (Rubio et al., 2018). The lack of oxidative stress associated to the exposure of PSNPs was confirmed by the studies of gene expression. Thus, not significant changes in the expression of the three ROS-related genes analysed (*HO1, GSTP1,* and *SOD2*) were detect, In addition, the lack of changes in the expression of the *HSP70* gene, which is an indicator of general cellular stress, would confirm the lack of toxicity associated to PSNPs exposure.

Another potential effect associated with MNPLs exposure is their ability to interact, directly or indirectly, with DNA producing genotoxic damage. It must be remembered that the confocal figures showed the presence of PSNPs inside the nucleus. This nuclear internalization was real because could be detected through sequential cuts that permits to discriminate if the particle is inside or just outside the nuclear membrane. Talking about the potential effects on humans associated to MNPLs exposure, the detection of genotoxicity is of paramount relevance because it has important implications for human health contributing to cancer, certain human diseases, and aging (Chatterjee and Walker, 2017). Our results indicate that PSNPs have not genotoxic potential , as demonstrated in the comet assay, what would agree with the inability to induce intracellular ROS. It must be remembered that ROS interact with DNA producing different types of damage, including 8-oxodG adducts. To detect this type of lesion we used the FPG enzyme that specifically identify this type of lesion, but not oxidized DNA bases were detected. In spite of the relevance of this biomarker few studies have been addressed to evaluate this effect and none using Caco-2 cells. Thus, this study is the only one that has evaluated the genotoxic damage induced by MNPLs on the gut cells.

In mammalian cells, the genotoxicity of fluorescent 50 nm PSNPs nanoparticles, with different functionalized surfaces (non-functionalized, carboxylated and aminated), was assessed using the γ-H2Ax foci assay. This assay permits specifically the detection of DNA double strand breaks. The study was performed in pulmonary epithelial cells (Calu-3) and in macrophages (THP-1).The obtained results indicated that only aminated NPLs were able to significantly increase the levels of DNA damage (Paget et al. 2015). On the other hand, the potential genotoxicity of two sized (50 nm and 0.5 μm) COOH-modified PSMNPLs were analysed using two different assays, the p53 reporter gene assay and the micronucleus assay (Hesler et al., 2019). The first assay, using the HepG2CDKN1A-DsRed biosensor cell line, detect changes in the expression of the p53 protein. The micronucleus assay, carried out in CHO-K1 cells, detects the induction of chromosome breakage and/or alterations in the chromosome segregation. In spite of the strong capability of internalization, no genotoxic effects were detected in neither of the two used assay. These results would agree with those

previously reported using negatively charged carboxylated polystyrene and positively charged amino-modified polystyrene (NH2ePS) nanoparticles of three different diameters (50, 100 and 500 nm) on cancer HeLa cells and normal NIH 3T3 cells. In such study, although important internalization was observed, the MNPLs used have not effects on any of the components of the mitotic apparatus. In addition, no alterations in the normal cell division were detected (Liu et al., 2011). Although all these studies show that pristine MNPLs have not genotoxic potential, as previously indicated the association with persistent organic pollutants can support a real genotoxic risk, This has shown with MPLs from sand beaches where association with polycyclic aromatic hydrocarbons was detected. Although no toxicity on the rainbow trout liver cell line (RTLW-1) was observed for virgin MPLs, DNA damage in the comet assay was observed after exposure to four MPLs samples on the six tested. This point out the need of evaluate real environmental samples instead of commercial pristine samples.

Acknowledgements

J. Domenech was supported by a Predoctoral Fellowship (PIF) from the Universitat Autònoma de Barcelona. We thank Dr. Victor Puentes' group (Inorganic Nanoparticles Group, ICN2) for supplying the protocol to characterize PS nanoparticles.

Author contribution

CC, RM and AH planned the experiments. JD, CC, and LR carried out the experimental part. CC and JD analysed the data, carried out the statistical analysis, and prepared tables/figures. CC, JD, AH and RM wrote the final manuscript.

Conflict of interest statement

The authors declare that there is no conflict of interest.

References

1. PlasticsEuropePlastics -The Facts 2017: Analysis of European plastics production, demand and waste data. PlasticsEurope, Belgium (2017), https://www.plasticseurope.org/application/files/5715/1717/4180/Plastics_the_facts_2017_FINAL_for_website_one_page.pdf.
2. Li WC, Tse HF, Fok L. Plastic waste in the marine environment: A review of sources, occurrence and effects. Sci Total Environ. 2016 566-567: 333-349.
3. M. Eriksen, N. Maximenko, M. Thiel, A. Cummins, G. Lattin, S. Wilson, J. Hafner, A. Zellers, S. Rifman. Plastic pollution in the South Pacific subtropical gyre. Mar. Pollut. Bull., 68 (2013), 71-76.
4. S. Lambert and M. Wagner, Formation of microscopic particles during the degradation of different polymers, *Chemosphere,* 2016, **161**, 510-517.
5. C. Ioakeimidis, K.N. Fotopoulou, H.K. Karapanagioti, M. Geraga, C. Zeri, E. Papathanassiou, F. Galgani and G. Papatheodorou, The degradation potential of PET bottles in the marine environment: An ATR-FTIR based approach, *Sci. Rep.,* 2016, **6**, 23501.
6. V. Hidalgo-Ruz, L. Gutow, R.C. Thompson and M. Thiel, Microplastics in the marine environment: a review of the methods used for identification and quantification, *Environ. Sci. Technol.,* 2012, **46(6)**, 3060-3075.
7. B. Silva, A.S. Bastos, C.I.L. Justino, J.P. da Costa, A.C. Duarte and T.A.P. Rocha-Santos, Microplastics in the environment: Challenges in analytical chemistry -A review, *Anal. Chim. Acta.,* 2018, **1017**, 1-19.
8. Carbery M, O'Connor W, Palanisami T. Trophic transfer of microplastics and mixed contaminants in the marine food web and implications for human health. Environ Int. 2018 115: 400-409.
9. Alimba CG, Faggio C. Microplastics in the marine environment: Current trends in environmental pollution and mechanisms of toxicological profile. Environ Toxicol Pharmacol. 2019 May;68:61-74.
10. Wright SL, Kelly FJ. Plastic and Human Health: A Micro Issue? Environ Sci Technol. 2017 51(12) :6634-6647.
11. S. Rist, B. Carney Almroth, N.B. Hartmann and T.M. Karlsson, A critical perspective on early communications concerning human health aspects of microplastics, *Sci. Total Environ.,* 2018, **626**, 720-726.
12. J.C. Prata. Airborne microplastics: consequences to human health? Environ. Pollut., 234 (2018), pp. 115-126.
13. Klein M, Fischer EK. Microplastic abundance in atmospheric deposition within the Metropolitan area of Hamburg, Germany. Sci Total Environ. 2019 May 29;685:96-103.
14. Sambuy, Y., De Angelis, I., Ranaldi, G., Scarino, M.L., Stammati, A., Zucco, F., 2005. The Caco-2 cell line as a model of the intestinal barrier: influence of cell and culture-related factors on Caco-2 cell functional characteristics. Cell Biol. Toxicol. 21, 1-26.
15. Araújo, F., Sarmento, B., 2013. Towards the characterization of an *in vitro* triple co-culture intestine cell model for permeability studies. Int. J. Pharm. 458, 128-134.
16. Lozoya-Agullo, I., Araújo, F., González-Álvarez, I., Merino-Sanjuán, M., González-Álvarez, M., Bermejo, M., Sarmento, B., 2017. Usefulness of Caco-2/HT29-MTX and Caco-2/HT29-MTX/Raji B coculture models to predict intestinal and colonic permeability compared to Caco-2 monoculture. Mol. Pharm. 14, 1264-1270.

17. Kucharzik, T., Lügering, N., Rautenberg, K., Lügering, A., Schmidt, M.A., Stoll, R., Domschke, W., 2000. Role of M cells in intestinal barrier function. Ann. NY Acad. Sci. 915, 171-183.

18. des Rieux, A., Fievez, V., Théate, I., Mast, J., Préat, V., Schneider, Y.J., 2007. An *improved in vitro* model of human intestinal follicle-associated epithelium to study nanoparticle transport by M cells. Eur. J. Pharm. Sci. 30, 380-391.

19. García-Rodríguez, A., Vila, L., Cortés, C., Hernández, A., Marcos, R., 2018a. Effects of differently shaped TiO_2NPs (nanospheres, nanorods and nanowires) on the *in vitro* model (Caco-2/HT29) of the intestinal barrier. Part. Fibre Toxicol. 15: 33.

20. García-Rodríguez A, Vila L, Hernández A, Marcos R. 2018b. Exploring the usefulness of the complex *in vitro* intestinal epithelial model Caco-2/HT29/Raji-B in nanotoxicology. Food Chem. Toxicol. 113: 162-170.

21. Toussaint B, Raffael B, Angers-Loustau A, Gilliland D, Kestens V, Petrillo M, Rio-Echevarria IM, Van den Eede G. 2019. Review of micro- and nanoplastic contamination in the food chain. Food Addit Contam Part A Chem Anal Control Expo Risk Assess. 36: 639-673.

22. Carbery M, O'Connor W, Palanisami T. 2018. Trophic transfer of microplastics and mixed contaminants in the marine food web and implications for human health. Environ Int. 115: 400-409.

23. Santana MFM, Moreira FT, Turra A. 2017. Trophic transference of microplastics under a low exposure scenario: Insights on the likelihood of particle cascading along marine food-webs. Mar Pollut Bull. 121: 154-159.

24. Auta HS, Emenike CU, Fauziah SH. 2017. Distribution and importance of microplastics in the marine environment: A review of the sources, fate, effects, and potential solutions. Environ Int. 102: 165-176.

25 Su L, Deng H, Li B, Chen Q, Pettigrove V, Wu C, Shi H. The occurrence of microplastic in specific organs in commercially caught fishes from coast and estuary area of east China. J Hazard Mater. 2019, 365: 716-724.

26. Kucharzik T, Lügering N, Rautenberg K, Lügering A, Schmidt MA, Stoll R, Domschke W. Role of M cells in intestinal barrier function. Ann N Y Acad Sci. 2000; 915: 171-183.

27. Magrì, D., P. Sánchez-Moreno, G. Caputo, F. Gatto, M. Veronesi, G. Bardi, G., T. Catelani, D. Guarnieri, A. Athanassiou, P. P. Pompa, D. Fragouli. 2018. Laser ablation as a versatile tool to mimic polyethylene terephthalate nanoplastic pollutants: Characterization and toxicology assessment. *ACS Nano*. 12: 7690-7700.

28. Wu, B., X. Wu, S. Liu, Z. Wang, and L. Chen. 2019. Size-dependent effects of polystyrene microplastics on cytotoxicity and efflux pump inhibition in human Caco-2 cells. *Chemosphere*. 221:333–341.

29. Stock, V., L. Böhmert, E. Lisicki, R. Block, J. Cara-Carmona, L. K. Pack, R. Selb, D. Lichtenstein, L. Voss, C.J. Henderson, E. Zabinsky, H. Sieg, A. Braeuning, A. Lampen A.. 2019. Uptake and effects of orally ingested polystyrene microplastic particles in vitro and in vivo. *Archives of Toxicology*. 93: 1817–1833.

30. Hesler M, Aengenheister L, Ellinger B, Drexel R, Straskraba S, Jost C, Wagner S, Meier F, von Briesen H, Büchel C, Wick P, Buerki-Thurnherr T, Kohl Y. Multi-endpoint toxicological assessment of polystyrene nano- and microparticles in different biological models in vitro. Toxicol In Vitro. 2019, 61: 104610.

31. Schirinzi, G. F., I. Pérez-Pomeda, J. Sanchís, C. Rossini, M. Farré, and D. Barceló. 2017. Cytotoxic effects of commonly used nanomaterials and microplastics on cerebral and epithelial human cells. *Environmental Research*. 159:579–587..

32. Lim SL, Ng CT, Zou L, Lu Y, Chen J, Bay BH, Shen HM, Ong CN. Targeted metabolomics reveals differential biological effects of nanoplastics and nanoZnO in human lung cells. Nanotoxicology. 2019, 13(8): 1117-1132.

33. Lin W, Jiang R, Wu J, Wei S, Yin L, Xiao X, Hu S, Shen Y, Ouyang G. Sorption properties of hydrophobic organic chemicals to micro-sized polystyrene particles. Sci Total Environ. 2019, 690: 565-572.

34. Bradney L, Wijesekara H, Palansooriya KN, Obadamudalige N, Bolan NS, Ok YS, Rinklebe J, Kim KH, Kirkham MB. Particulate plastics as a vector for toxic trace-element uptake by aquatic and terrestrial organisms and human health risk. Environ Int. 2019 131: 104937.

35. Alimba CG, Faggio C. Microplastics in the marine environment: Current trends in environmental pollution and mechanisms of toxicological profile. Environ Toxicol Pharmacol. 2019, 68: 61-74.

36. Rubio L, Marcos R, Hernández A. Nanoceria acts as antioxidant in tumoral and transformed cells. Chem Biol Interact. 2018, 291:7-15

37. Chatterjee N, Walker GC. Mechanisms of DNA damage, repair, and mutagenesis. Environ Mol Mutagen. 2017 58(5):235-263.

38. Kawanishi S, Ohnishi S, Ma N, Hiraku Y, Murata M. Crosstalk between DNA Damage and Inflammation in the Multiple Steps of Carcinogenesis. Int J Mol Sci. 2017 19; 18(8).

39. Pannetier P, Cachot J, Clérandeau C, Faure F, Van Arkel K, de Alencastro LF, Levasseur C, Sciacca F, Bourgeois JP, Morin B. Toxicity assessment of pollutants sorbed on environmental sample microplastics collected on beaches: Part I-adverse effects on fish cell line. Environ Pollut. 2019 248: 1088-1097

FIGURE LEGENDS

Figure 1. Characterization of PSNPs by TEM. Representative TEM images of 100 µg/mL nPSNPs or y-nPSNPs dispersions in distilled H_2O or DMEM are presented.

Figure 2. Relative survival of Caco-2/HT29 monolayers and Raji-B cells after the exposure to nPSNPs for 24 h. A) Relative survival of the Caco-2/HT29 barrier after exposing the Caco-2/HT29 *in vitro* model to nPSNPs. B) Relative survival of the Caco-2/HT29 barrier and Raji-B cells after exposing the Caco-2/HT29 + Raji-B *in vitro* model to nPSNPs. The concentration of nPSNPs ranged from 0 to 200 µg/mL. Data are represented as the percentage of counted cells relative to the untreated control ± SEM.

Figure 3. nPSNPs effects on the Caco-2/HT29 barrier's integrity. TEER values after the exposure of the Caco-2/HT29 model (A) or after the exposure of the Caco-2/HT29 + Raji-B model to different concentrations of nPSNPs (B). Benzalkonium chloride (BNZ, 20 mg/mL) was used as a positive control in all three independent experiments carried out. All data are represented as mean ± SEM.

Figure 4. Percentage of LY in the basolateral chamber after nPSNPs exposure. 20 mg/mL benzalkonium chloride (BNZ) was used as a positive control as well as a cell-free insert (CF). Data represent the mean ± SEM of three independent experiments.

Figure 5. Three-dimensional images were taken by confocal microscopy to determine the y-nPSNPs location in the Caco-2/HT29 and Caco-2/HT29 + Raji-B models 24 h after the exposure. Nuclei (blue) were stained with Hoechst while cell membranes and the mucus layer (red) were stained with Cell Mask. y-nPSNPs are shown in green and some internalized y-nPSNPs inside the nuclei are pointed out with white arrows.

Figure 6. y-nPSNPs intake by Caco-2/HT29 barriers and Raji-B cells after 24 h of exposure. (A–C) Percentage of fluorescent-positive cells over the living cells total population from the Caco-2/HT29 barrier, Caco-2/HT29 (+ Raji-B) barrier, and Raji-B cells, respectively. (A'–C') Mean fluorescence emission of fluorescent-positive living cells from the Caco-2/HT29 barrier, Caco-2/HT29 (+ Raji-B) barrier, and Raji-B cells, respectively. Data are represented as mean ± SEM and analyzed by the student's t-test, comparing to the untreated control.

Figure 7. Relative analysis of the ROS production in Caco-2/HT29 monolayers belonging to the Caco-2/HT29 and Caco-2/HT29 + Raji-B *in vitro* models. Samples were exposed to nPSNPs for 24 h and the ROS production was analyzed using the DCFH-DA (A and B) and DHE (C and D) methods. H_2O_2 and CSC (cigarette smoke condensate) were used as positive controls, respectively. Data are represented as mean ± SEM and analyzed by the student's t test.

Figure 8. Genotoxic damage and oxidative DNA damage (ODD) observed in the Caco-2/HT29 monolayers of the Caco-2/HT29 (A and A', respectively) and Caco-2/HT29 + Raji-B (B and B', respectively) models, as assessed by the comet assay after 24 h of nPSNPs exposure. 200 µM MMS and 5 mM $KBrO_3$ were used as positive controls for genotoxic damage or ODD, respectively. Data are represented as mean ± SEM.

Figure 9. Relative mRNA expression analysis by Real-Time RT PCR of *HO1*, *GSTP1*, *SOD2* and *HSP70* genes. Caco-2/HT29 and Caco-2/HT29 + Raji-B *in vitro* models were exposed to 0-100 µg/mL nPSNPs for 24 h, and the expression of the genes in the monolayers was analyzed. Data are represented as mean ± SEM and analyzed by the Student's t-test.

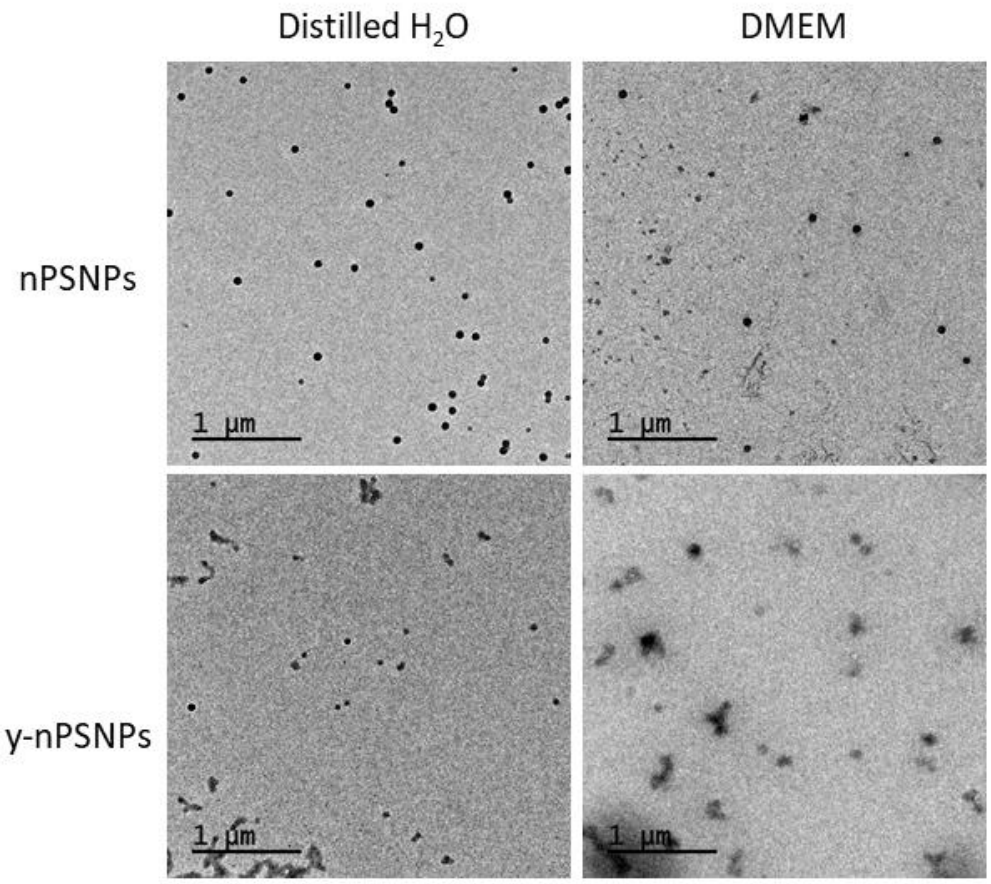

FIGURE 1

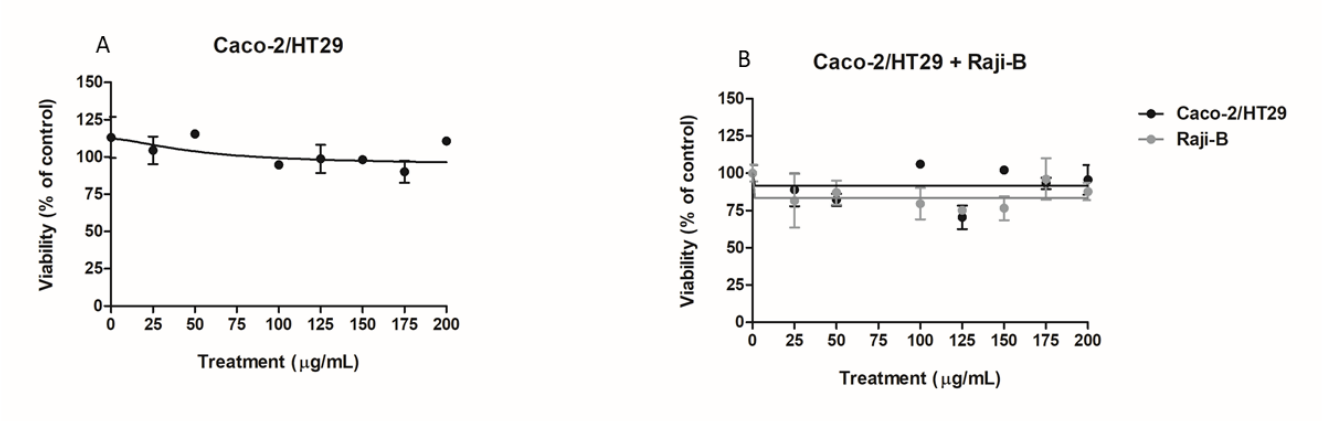
A
Caco-2/HT29
Viability (% of control)
Treatment (μg/mL)
B
Caco-2/HT29 + Raji-B
Caco-2/HT29
Raji-B
Viability (% of control)
Treatment (μg/mL)

FIGURE 2

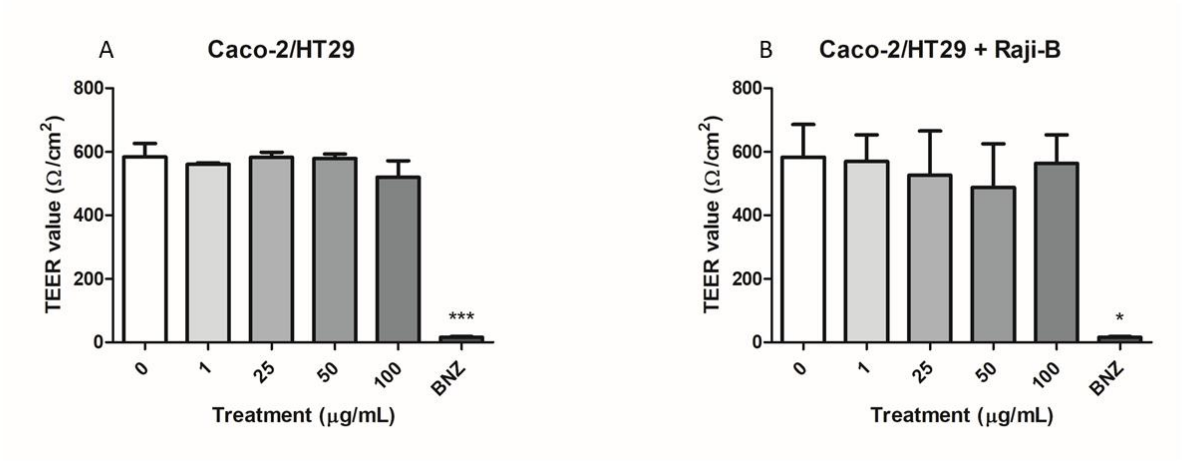
A
Caco-2/HT29
TEER value (Ω/cm²)
800
600
400
200
0
***
0
1
25
50
100
BNZ
Treatment (μg/mL)
B
Caco-2/HT29 + Raji-B
TEER value (Ω/cm²)
800
600
400
200
0
*
0
1
25
50
100
BNZ
Treatment (μg/mL)

FIGURE 3

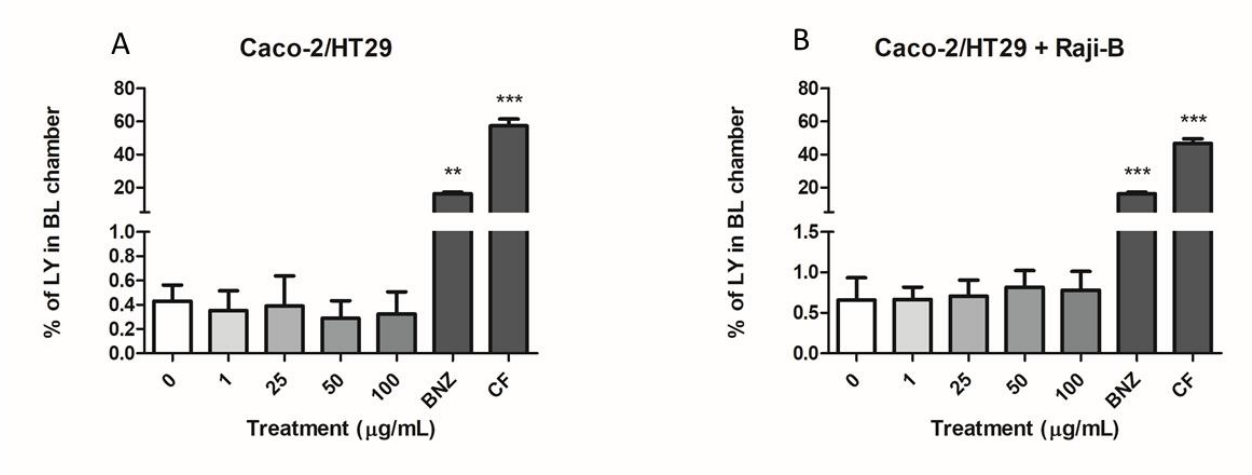
A
Caco-2/HT29
% of LY in BL chamber
80
60
40
20
1.0
0.8
0.6
0.4
0.2
0.0
**
***
0
1
25
50
100
BNZ
CF
Treatment (μg/mL)
B
Caco-2/HT29 + Raji-B
% of LY in BL chamber
80
60
40
20
1.5
1.0
0.5
0.0
***
***
0
1
25
50
100
BNZ
CF
Treatment (μg/mL)

FIGURE 4

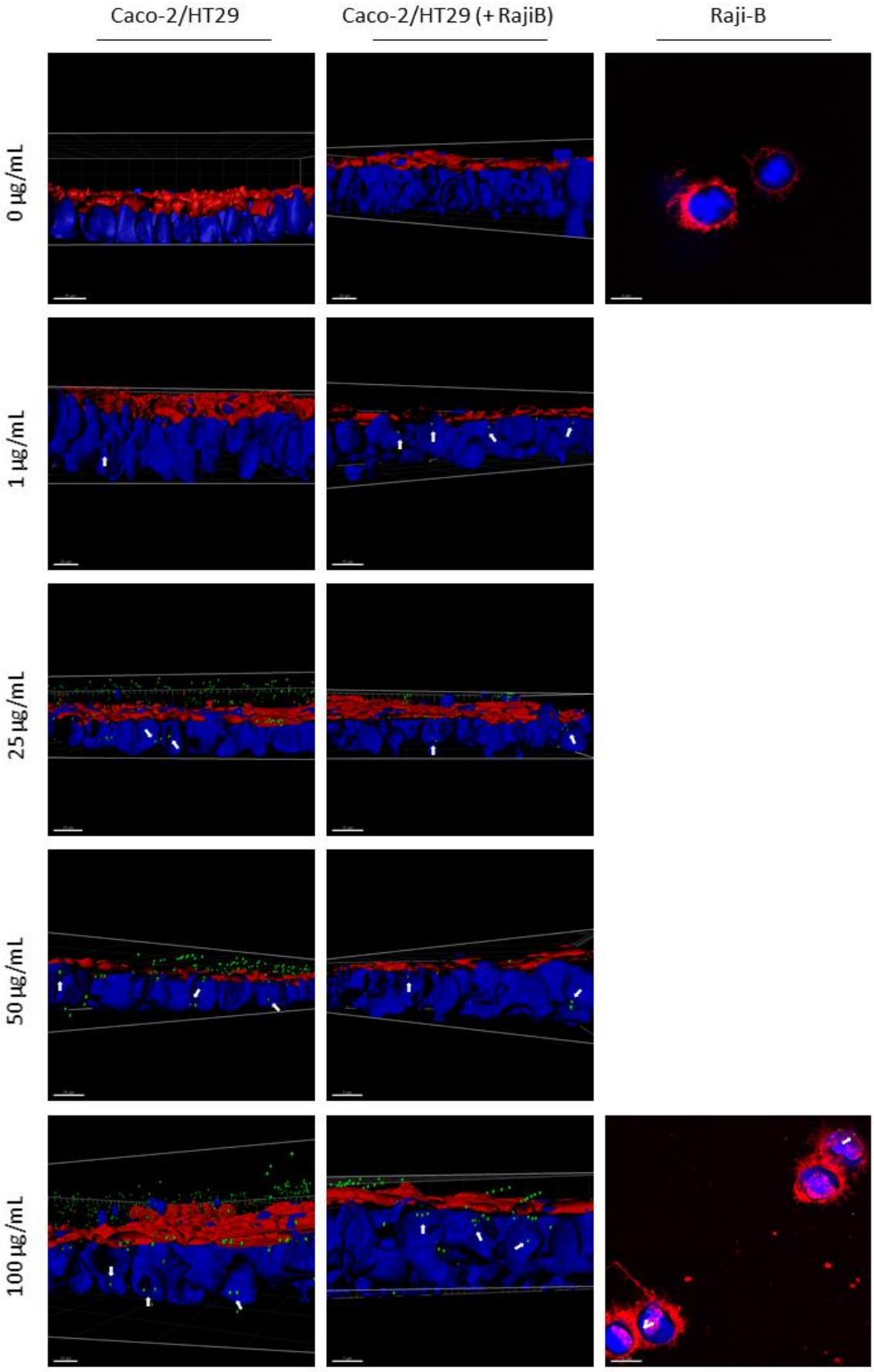
Caco-2/HT29
Caco-2/HT29 (+ RajiB)
Raji-B
0 µg/mL
1 µg/mL
25 µg/mL
50 µg/mL
100 µg/mL

FIGURE 5

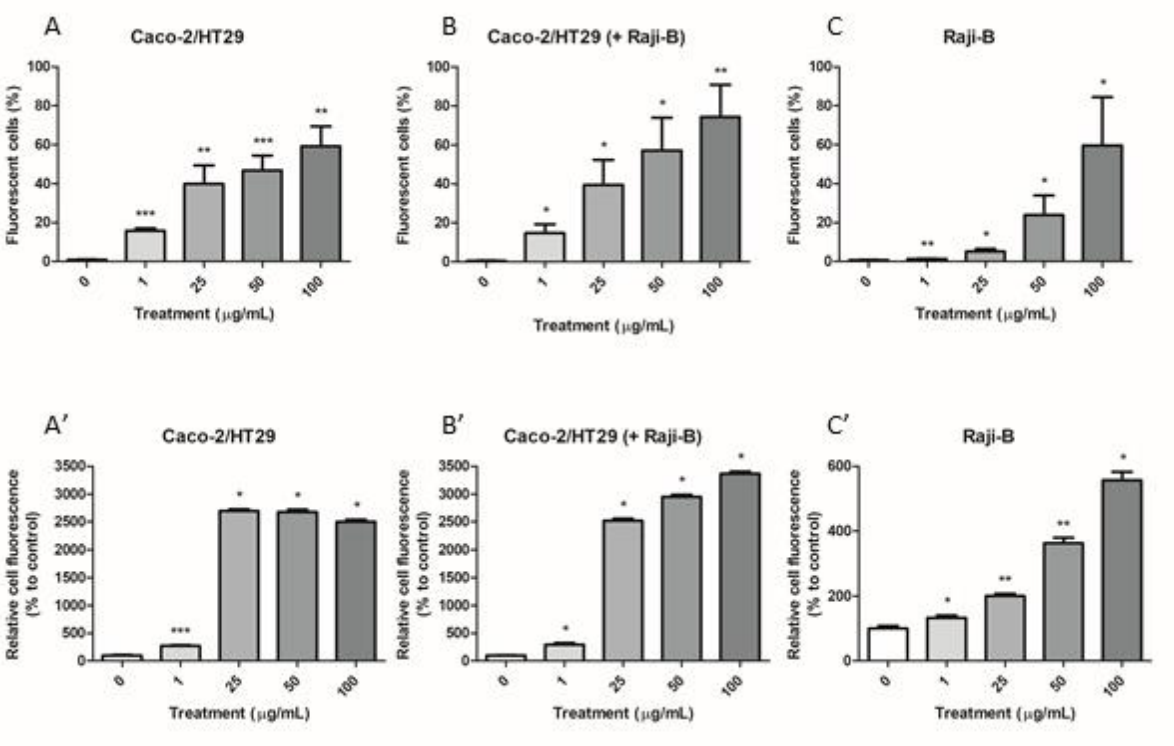

FIGURE 6

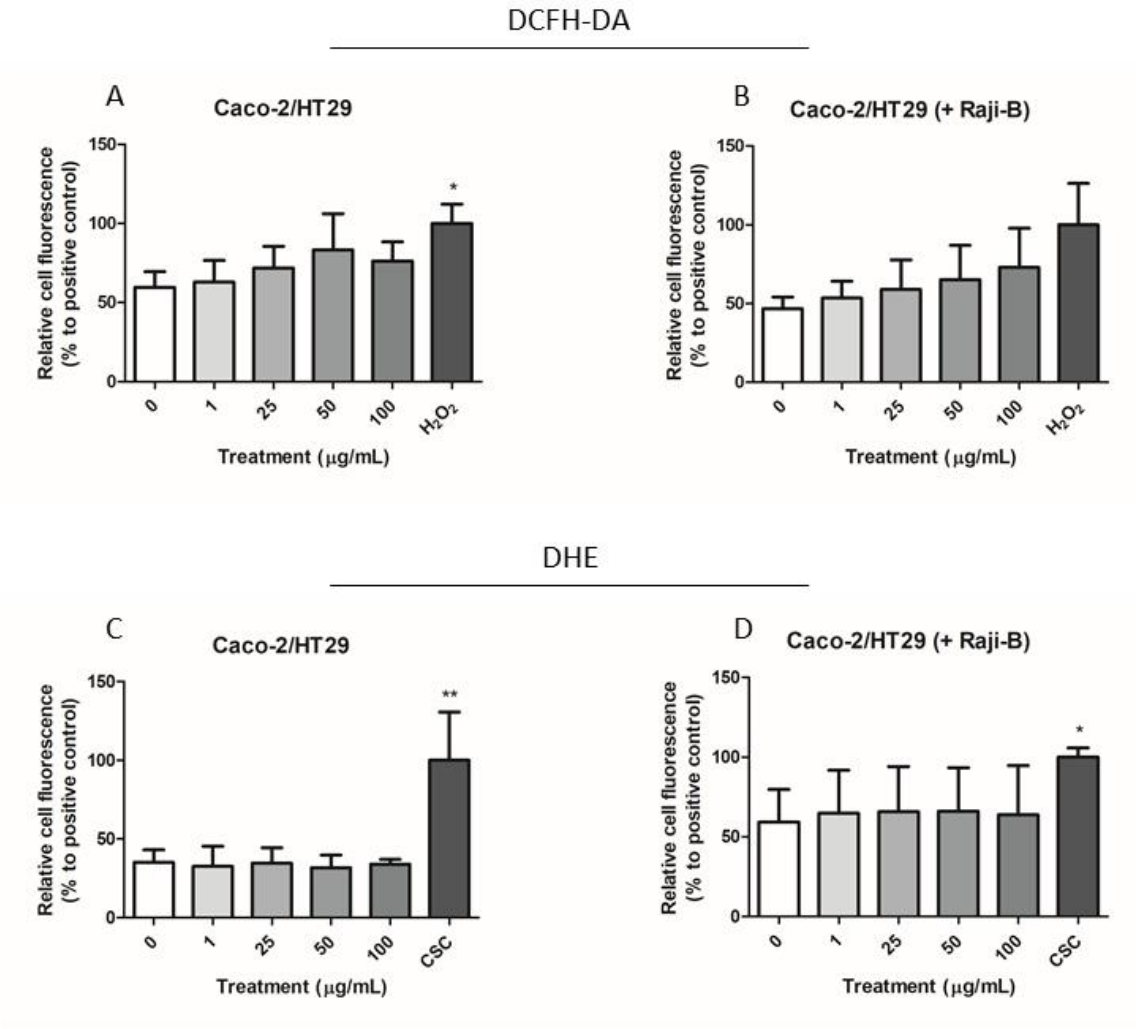
DCFH-DA
A
Caco-2/HT29
Relative cell fluorescence (% to positive control)
150
100
50
0
*
0
1
25
50
100
H2O2
Treatment (µg/mL)
B
Caco-2/HT29 (+ Raji-B)
Relative cell fluorescence (% to positive control)
150
100
50
0
0
1
25
50
100
H2O2
Treatment (µg/mL)
DHE
C
Caco-2/HT29
Relative cell fluorescence (% to positive control)
150
100
50
0
**
0
1
25
50
100
CSC
Treatment (µg/mL)
D
Caco-2/HT29 (+ Raji-B)
Relative cell fluorescence (% to positive control)
150
100
50
0
*
0
1
25
50
100
CSC
Treatment (µg/mL)

FIGURE 7

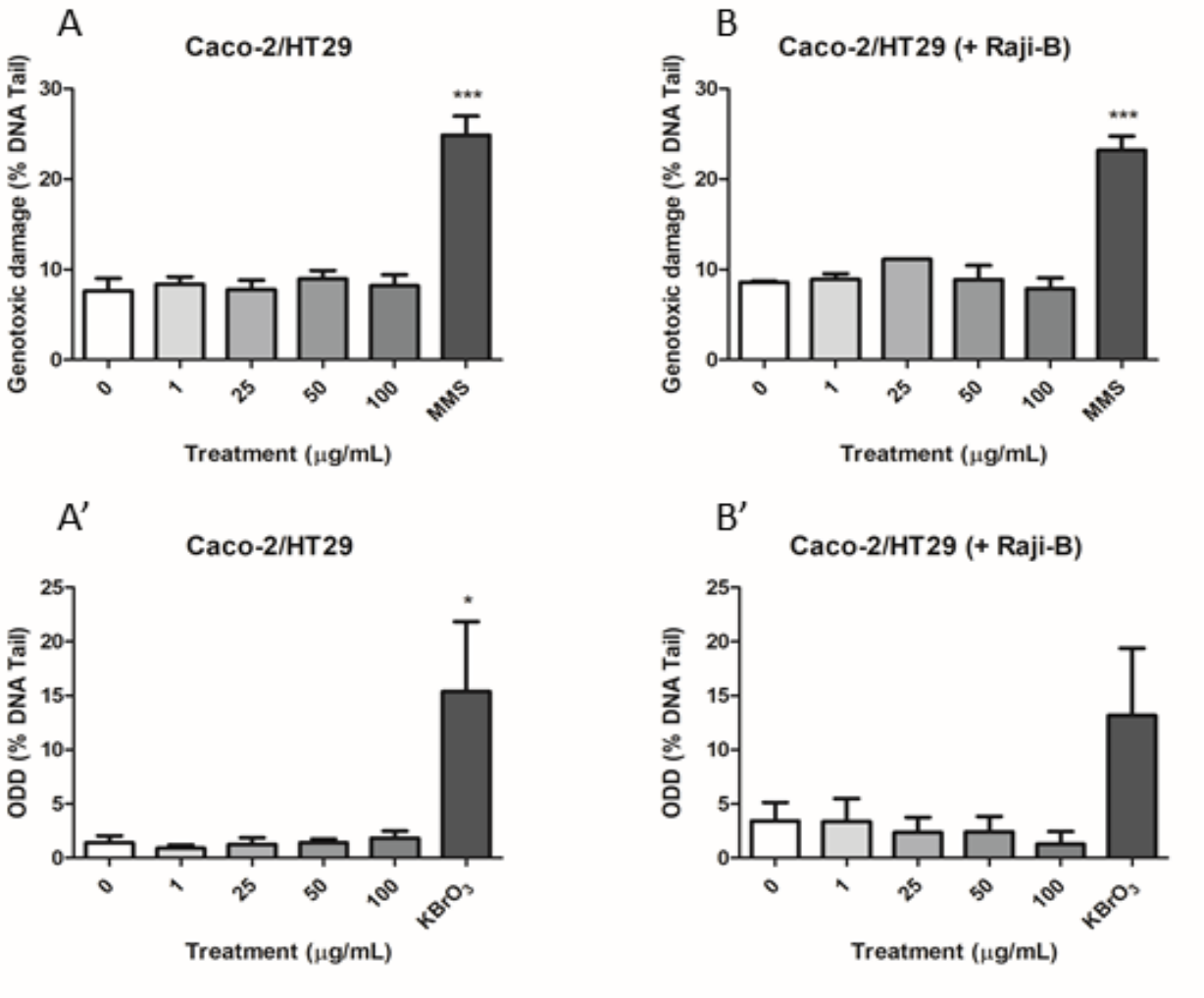
A
Caco-2/HT29
Genotoxic damage (% DNA Tail)
30
20
10
0
***
0
1
25
50
100
MMS
Treatment (μg/mL)
B
Caco-2/HT29 (+ Raji-B)
Genotoxic damage (% DNA Tail)
30
20
10
0
***
0
1
25
50
100
MMS
Treatment (μg/mL)
A′
Caco-2/HT29
ODD (% DNA Tail)
25
20
15
10
5
0
*
0
1
25
50
100
KBrO3
Treatment (μg/mL)
B′
Caco-2/HT29 (+ Raji-B)
ODD (% DNA Tail)
25
20
15
10
5
0
0
1
25
50
100
KBrO3
Treatment (μg/mL)

FIGURE 8

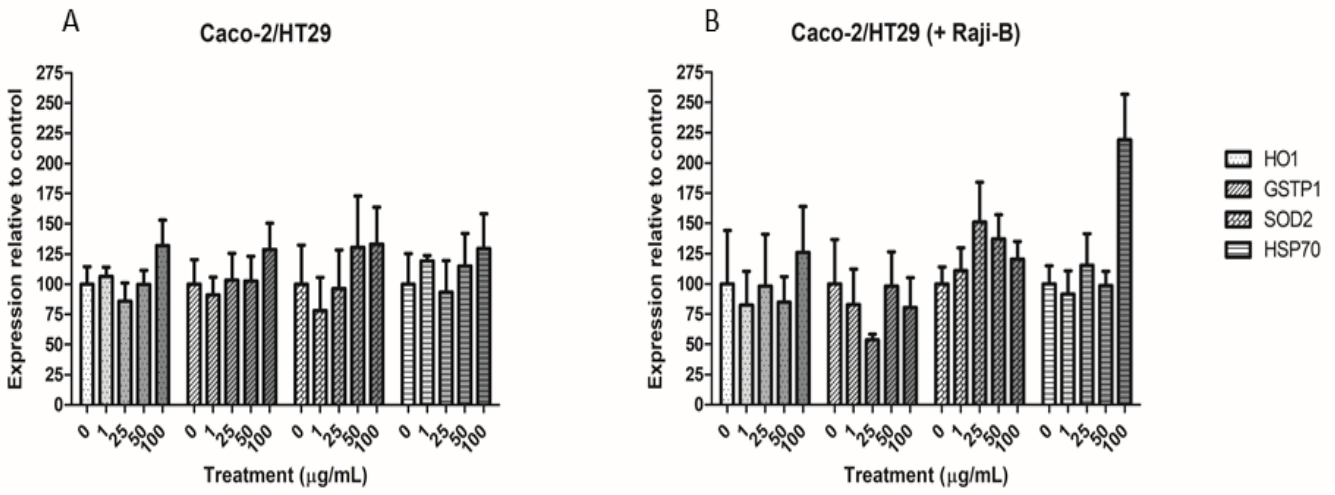
A
Caco-2/HT29
Expression relative to control
Treatment (µg/mL)
B
Caco-2/HT29 (+ Raji-B)
Expression relative to control
Treatment (µg/mL)
HO1
GSTP1
SOD2
HSP70

FIGURE 9

Table 1. Forward and reverse 5´-3´ primer sequences of the genes analyzed by Real-Time RT PCR.

Gene	Forward	Reverse
HO1	5'-TCCGATGGGTCCTTACACTC-3'	5'-AAGGAAGCCAGCCAAGAGA-3'
GSTP1	5´-CCAATACCATCCTGCGTCAC-3´	5´-CAGCAAGTCCAGCAGGTTGT-3´
HSP70	5'-TGATCAACGACGGAGACAAG-3'	5'-TCCTTCATCTTGGTCAGCAC-3'
SOD2	5´-GGCCTACGTGAACAACCTGA-3´	5´-GAGCCTTGGACACCAACAGA-3´
β-actin	5´-GCATGGAGTCCTGTGGCATC-3´	5´-CCACACGGAGTACTTGCGCT-3´

Table 2. PS nanomaterials characterization by TEM and Zetasizer Nano ZS.

	nPSNP		**y-nPSNP**	
Dispersant	Distilled H_2O	DMEM	Distilled H_2O	DMEM
Size (nm) (TEM)	52.99 ± 14.68	48.59 ± 16.38	44.19 ± 28.54	55.21 ± 12.76
Size (nm) (DLS)	86.33 ± 10.20	158.28 ± 10.85	112.87 ± 3.11	377.52 ± 43.05
PdI (DLS)	0.10 ± 0.09	0.44 ± 0.09	0.35 ± 0.02	0.60 ± 0.06
Z-potential (mV) (DLV)	-36.00 ± 7.88	-9.31 ± 0.67	-45.97 ± 3.84	-9.80 ± 0.33
Mobility (μm cm/Vs) (DLV)	-2.29 ± 0.10	-0.71 ± 0.05	-3.76 ± 0.38	-0.74 ± 0.03